Infinite Science | Publishing

Numerical simulation of multimaterial polymer mixing for bioprinting applications

G. Ates[1], P. Bartolo[1*]

[1] *School of Mechanical, Aerospace and Civil Engineering, The University of Manchester, Manchester, UK*
[*] *Corresponding author, email: paulojorge.dasilvabartolo@manchester.ac.uk*

Abstract

In tissue engineering, three-dimensional (3D) functional constructs (cellular or acellular) with tailored biological properties are needed to be able to mimic the hierarchical structure of biological tissues. Recent developments in extrusion based additive manufacturing considerably improved the ability to fabricate sophisticated tissue constructs by allowing to extrude multiple materials through different printing heads. This paper investigates the flow behavior of two miscible biomaterials inside an extrusion chamber incorporated with a Kenics static mixer (KSM). A computational fluid dynamics (CFD) model for isothermal non-Newtonian fluid flow was developed to numerically analyze the flow behavior of the fluids. The power-law model was used to characterize the shear-thinning behavior of the studied biomaterials. The mixing performance of designed chamber was also investigated by varying the inlet angles and velocities as well as the effect of the number of mixing units, pseudoplastic behavior of fluids, and pressure drop throughout the fluid domain. The results indicated that the inlet angle did not have a significant impact on the mixing quality and the proposed mixing channel showed good mixing performance regardless of the inlet velocities. The mixing index increases by increasing the power-law index and the shear-thinning behavior decreases the pressure drop value compared to Newtonian fluids.

Keywords: Bioprinting, CFD, Multi-material, 3D-printing, Mixing index

1. Introduction

3D bioprinting allows to print a wide range of hydrogel-based materials containing cells and growth-factors for the fabrication of complex tissue-like structures [1]. This technology comprises three main techniques[2]: laser-assisted printing [3], inkjet printing [4], and material extrusion bioprinting [5]. Among these strategies, extrusion based bioprinting is the most widely used approach due to its printing speed [6], high efficiency and ability to process a wide variety of biomaterials [6,7].

The bioprinting of tissue engineering requires the use of multiple materials since a single material cannot mimic the functional complexity of a tissue [8]. Current multi-material biofabrication and bioassembly technologies enable to create relatively complex lamellar structures, however, placing different cell types next to each other with high resolution and in a cost-effective manner is still challenging [9]. Current additive bioprinting systems address this limitation has they incorporate multiple printheads and, in some cases, different printing technologies to produce multi-material tissue constructs [3,4]. Recent advances in the field include co-axial nozzles and material mixing systems which enable the development of core-shell or hollow fibres and gradient structures, respectively [3,5]. Due to the high potential and the development of hybrid biomanufacturing systems which incorporate multiple technologies, the fabrication of complex tissues and organs may come true. However, the flow characteristics of potential hydrogels for extrusion based bioprinting and the mixing capability of the designed printing heads have not been extensively studied in the literature. Determining the flow behaviour of a bioink (hydrogel containing cells) flowing through a nozzle is highly important to optimise the printing process but cannot be easily achieved through experimental tests. The main reason for that is the dimensions of the nozzles that are usually small in size and difficult to sensorize. Therefore, experimental studies mostly focuses on the results of biofabrication such as cell viability, fibre shape fidelity, or printability rather than the process parameters including pressure drop, velocity and shear stress during the printing process [6]. In order to successfully achieve optimised printed tissue structures the printing parameters need to be carefully adjusted [7]. However, a trial and error approach is far from ideal and results into a waste of time and material [10]. In this sense, computational fluid dynamics (CFD) simulation arises as an important tool to carry out series of parametrical studies [11]. CFD analyses enable to determine certain microfluids inner parameters that are difficult to measure by experiments (i.e., shear stress, velocity, and pressure drop). Some numerical studies were already performed to investigate the flow behaviour of bioink during the extrusion process [9, 10, 12-14]. However, these studies considered the biomaterials as Newtonian or generalized Newtonian fluids for simplicity.

In the context of 3D bioprinting, a CAD model of a

printhead equipped with a KSM, which consists of multiple helicoidal elements, was designed to achieve better homogenization of different materials. This mixer type leads to a lower pressure drop than the other types of static mixers [15] and it maintains a constant cross-section throughout the channel, which is an efficient way to avoid clogging [16].

In this study, flow characteristics of the widely used non-Newtonian shear-thinning biomaterials, alginate and gelatin, were computationally investigated. The numerical analysis was performed on printheads with KSM and without any mixing elements inside the chamber to determine the contribution of inlet angle on mixing quality. The results were evaluated in terms of critical parameters such as mixing index, pressure drop, and velocity as well as the capability of creating functionally graded structures by manipulating the composition of materials through different flow rates applied from each inlet. The obtained values provided significant information regarding the mixing behaviour of the materials, velocity field, pressure drop and the ability to create homogenous functionally graded structures before moving on the experimental work.

2. Numerical Model

Numerical analysis was carried out using ANSYS CFX 19.2 (ANSYS Inc, USA) to evaluate the flow behaviour of biomaterials inside the printhead. It should be noted that the chaotic printer model containing a KSM is simulated for different inlet velocities ranging from 10 mm/s to 2000 mm/s. Due to the presence of mixing units, a transition from steady to unsteady state occurs at relatively low Reynolds numbers in the KSM included printhead (Re≈300) [17]. Here, the calculated maximum Reynolds number is less than 300 for all cases. Multicomponent, steady-state, laminar, incompressible, and isothermal non-Newtonian flow conditions without any reaction were considered in all simulations.

2.1. Mathematical equations

The Kenics mixer is one of the most widely investigated static mixer for both laminar and turbulent flow regime [18,19]. The mathematical model of the multi-component and non-Newtonian fluids is given by the Navier-stokes equations. In the case of an incompressible flow, the volume continuity, momentum conservation and transport equations are expressed as follows:

$$\nabla . \, u = 0 \tag{1}$$

$$\nabla . \, (\rho uu) = -\nabla p + \nu \nabla^2 u \tag{2}$$

$$(u. \nabla)C = \alpha \nabla^2 C \tag{3}$$

where u us the fluid velocity (m/s), α is the kinematic diffusivity coefficient, and C is the concentration of one of the fluids mixed in the static mixer, ρ is the fluid density (kg/m^3), and p represents the pressure (Pa).

For non-Newtonian fluid flows, the apparent viscosity and the shear rate are calculated using the power law model which accurately describes shear thinning fluids [18]:

$$\eta = k \, \dot{\gamma}^{n-1} \tag{4}$$

the shear rate $(\dot{\gamma})$, can be defined as follows:

$$\dot{\gamma} = \frac{d_u}{d_r} = \frac{-\Delta P}{2\mu L} r \tag{5}$$

where n is the power-law index (dimensionless), k is the fluid consistency coefficient (Pa.s^n), and u is the velocity of flow (mm) at the pipe with radius r (mm). According to [19], the generalized Reynolds number for a shear thinning fluid (Power-law model) is described as:

$$Re = \frac{\rho u^{2-n} D^n}{\frac{k}{8} \left(\frac{6n+2}{n} \right)^n} \tag{6}$$

Where D denotes the pipe diameter (mm).

2.2. Mixing index calculation

The distributive mixing capacity of the printhead was analysed for different inlet velocities within the laminar region. As the distributive mixing capacity of a mixer cannot be judged depending on the visual contour plots only, it is essential to quantitatively evaluate the mixing performance [20]. Therefore, the mixing efficiency of the static mixer was analysed using a statistical measurement method based on the concept of intensity of segregation. As previously reported, the mixing processes can be quantified using the mixing index (MI) at a cross-sectional plane perpendicular to flow direction, according to the following equation [1–6]:

$$M.I = \sqrt{\frac{\sigma^2}{\sigma_{max}^2}} \tag{7}$$

where σ^2 refers to the actual variance, σ_{max}^2 denotes maximum possible variance at a cut-plane normal to the flow direction and σ^2 is defined as:

$$\sigma^2 = \frac{1}{n} \sum_{i=1}^{n} (c_i - \bar{c})^2 \tag{8}$$

where c_i is the mass fraction at ith sampling point, $\bar{c}$ is the optimal mixing mass fraction and n is the number of sampling points on the associated plane. The optimal mass fraction $(\bar{c})$ at the cut plane is equal to 0.5 for symmetrical boundary conditions. The maximum variance (σ_{max}^2) can be determined as follows:

$$\sigma_{max}^2 = \bar{c}(1 - \bar{c}) \tag{9}$$

As the optimal maximum mass fraction $\bar{c}$ is equal to 0.5, in the case of equal flow of the fluid streams the value of

Infinite Science | Publishing

σ_{max}^2 is considered to be equal to 0.25. The mixing index varies from 0 (unmixed state) to 1 (completely mixed fluid). Moreover, as the mixing index decreases from 1 to 0, a lesser amount of mixing is achieved. Conversely, the higher mixing index represents higher mixing performance. However, it has been reported that the numerical results might overestimate the mixing quality due to numerical diffusion [21].

2.3. Numerical simulations

Fig. 1 shows the flow domain of the printhead equipped with a KSM, which consists of a series of blades of alternating clockwise and counter-clockwise twist arranged axially within a bifurcated pipe so that the leading edge of a blade is at the right angles to the following edge of the previous blade. Therefore, Kenics blades are usually designed with a twist angle of 180° and a rotation angle of 90° relative to the previous element [22,23].
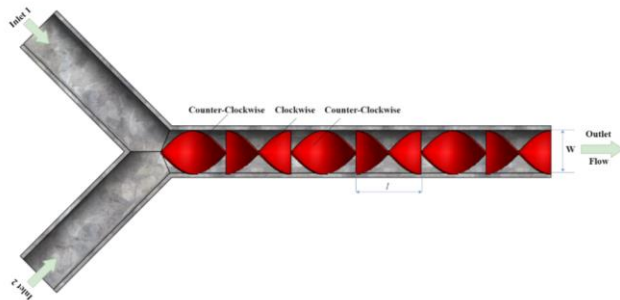

Fig 1. The flow domain of the printhead equipped with a KSM which consists of two inlets and one outlet.

The geometric parameters of the KSM are presented in Table 1.

Table 1. Geometric parameters of the Kenics mixer.

Geometrical Parameter	Kenics Static Mixer
Pipe Diameter, W (m)	0.005
Blade length, l (m)	0.075
Blade width, w (m)	0.005
Blade thickness, δ (m)	0.0005
Aspect Ratio, Ar	1.5
Twist angle, θ (deg)	180
Angle between inlets, θ (deg)	90
Inlet entrance lengths, li (m)	0.04
Mixing zone length, lm (m)	0.09

To solve the governing equations in the case of a laminar flow, the following conditions were considered:

- Uniform and fully developed velocity profiles were introduced from the inlets and the velocity values are fixed for each fluid.

- The rheological properties of the considered materials (alginate and gelatin) were obtained from the literature [24,25], see Table 2.
- The non-gelled alginate solution enters through the inlet 1, while the non-gelled gelatin solution enters at the inlet 2.
- The static pressure was set to zero at the outlet.
- The no-slip condition was applied at the walls.
- As the software only requires the diffusivity coefficient for one material, a low diffusivity coefficient of 1×10^{-11} was assumed for alginate so that the molecular diffusion can be neglected. Hence, the mixing process is considered to take place only by convection.

Table 2. Rheological parameters of alginate and gelatin.

Hydrogel	Content %	k(Pa.s^n)	n
Alginate	2	2	0.87
	3	6	0.84
	5	28	0.84
Gelatin	5	39.17	0.084

The flow domain was discretized using unstructured tetrahedral elements. To discretize the advection terms, a high-resolution scheme of second-order approximation was employed. A converge criterion of root-mean-square (RMS) residual value of 1.0×10^{-6} was established, and the number of iterations was set to 5000.

3. Results and discussion

Numerical simulations were carried out to address the flow characteristics of the biomaterials exhibiting shear thinning behaviour inside the printing head. The effect of various parameters such as inlet angle, inlet velocity and the number of mixing units, the shear-thinning behaviour, pressure drop, and unequal inlet bulk velocities were examined.

3.1. Effect of the inlet angle on the mixing quality

Before numerically analysing the proposed printhead composed of a KSM, it was important to investigate the effect of the inlet angle considering pipes without mixing elements. This allows to determine the effect of the inlet angle on the mixing performance. Four different angles between the two inlet channels were considered (60^0, 90^0, 180^0, and 270^0) as shown in Fig. 2. In all cases, the non-Newtonian power-law model was set using the rheological properties of 5% alginate and 5% gelatin solutions presented in Table 2. The inlet velocity for both materials was assumed to be 100 mm/s. The influence of straight channel inlet angle on the mass fraction distributions of the fluids were evaluated by plotting mass fraction contours at successive cross-sectional planes across the mixing zone. The mass fraction at the inlets was considered as the reference for the calculations, a step function was

observed through the mixing channel width, with half of the bifurcated pipe filled with gelatin solution (blue colour) and the other with alginate (red colour), as shown in Fig. 2. As observed fluid interfaces, throughout the straight channel outlet, were generated for all considered cases. Fig. 2 also shows the contour plots for the cross-sectional planes at the outlet. Results show that the mixing phenomenon only occurs at the interfacial area where the colours turn to green, and it indicates poor mixing quality.

As previously indicated, the mixing performance of static mixers cannot only be determined based on visual contour plots. Therefore, to quantitatively assess uniformity or the degree of mixing, the mixing index was determined at the outlet cross sections. The calculated MI values at the outlet of each mixing channel are indicated in Fig. 2. Based on the mixing index values, it is possible to observe that all types of mixing chambers with varying inlet angles exhibit similar mixing performance - MI of 0.29 for 60^0, 90^0 and 180^0 and 0.27 for the 270^0 inlet angle. These findings suggest that, for a mixing chamber of this scale, the inlet angle does not have a significant effect on the mixing quality. These results are similar to those reported by [26] for a T-mixer.
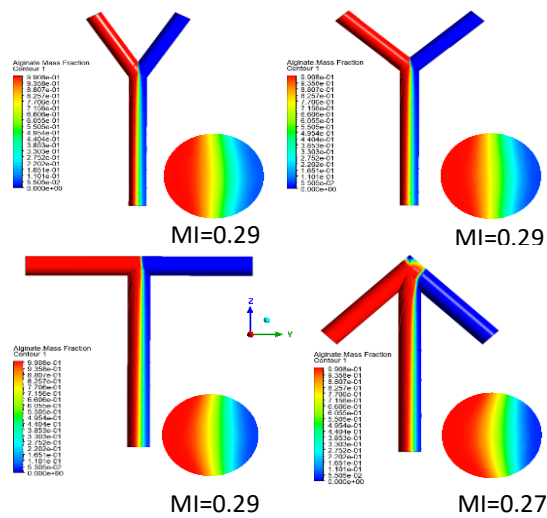

Fig 2. Alginate mass fraction distribution across the mixing channels with different inlet angles: a) 60^0; b) 90^0; c) 180^0; d) 270^0.

3.2. Effect of inlet velocity and number of mixing units on the mixing process

To investigate the effect of the fluid velocities on the mixing performance of a KSM, a range of velocity values from 20 mm/s to 2000 mm/s were considered. In this case 5% alginate and 5% gelatin hydrogels were considered assuming the corresponding rheological parameters presented in Table 2. The non-Newtonian fluid properties have been set according to the Ostwald de Waele (power-law) model [18].

Fig. 3 presents the mixing index values as a function of the inlet velocities. As observed, the mixing index slightly increases as the velocity increases from 20

mm/s to 40 mm/s, reaches a plateau between 40 mm/s and 100 mm/s, and seems to decrease for high velocity values (2000 mm/s). This trend, can be attributed to the fact that low velocities result in long residential time of the fluids allowing for more time for diffusion [22, 40, 41]. However, for all considered velocities, the proposed static mixer showed a good mixing performance due to the presence of chaotic advection.
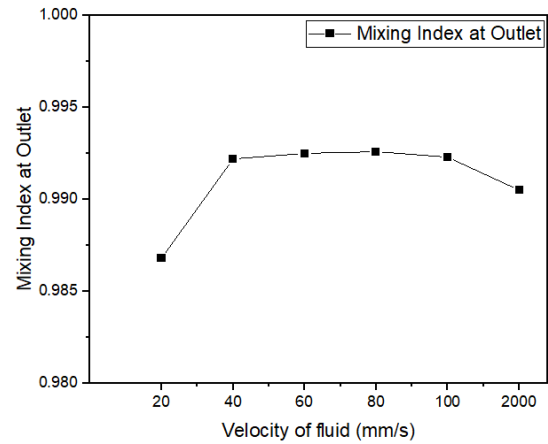

Fig 3. Effect of fluid velocity on the mixing index.

Fig. 4 shows the mass fraction contour plots for two different inlet velocities (20 mm/s and 2000 mm/s). Results show that as the two materials flows into the mixing zone, transverse dispersion occurs at the end of each mixing element due to stretching and folding mechanisms. The interfacial area becomes progressively blurred with the two materials mingled together through stretching, splitting, and recombining of the fluid-streams towards complete mixing at the end of the mixer.
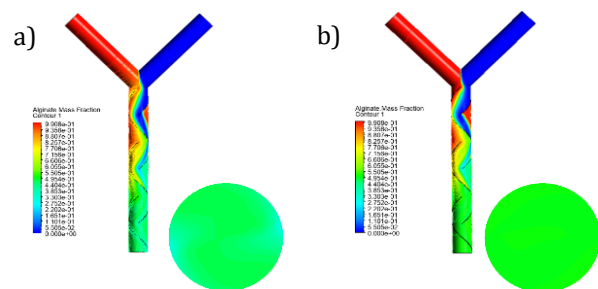

Fig 4. Alginate mass fraction (red colour) distribution across the mixer and at outlet cross-sections for two inlet velocities: (a) 20 mm/s, (b) 2000 mm/s.

The effect of the number of mixing units on the degree of mixing at different inlet velocities is presented in Fig. 5. Results show that the lowest mixing occurs at the cross-sectional plane where no mixing element is present. As the fluids proceed to the outlet, progressively uniform mass fraction distributions were accomplished, and the mixing index significantly increased. Results also show that once the flow passes the fourth mixing element (near the exit) the mixing index remains almost the same for all considered cases. Similar results have been also reported, suggesting that high quality of mixing can be achieved at the fourth or

fifth element near the inlet of a motionless mixer for nonreactive viscous fluids [21,22,27]. This phenomenon is defined as tailpipe or downstream effects in the literature. In the case of laminar flow, no further mixing takes place in this region. However, in the case of turbulent flow, the mixing conditions will continue to improve since the extra turbulence produced by the mixing units is removed [28].
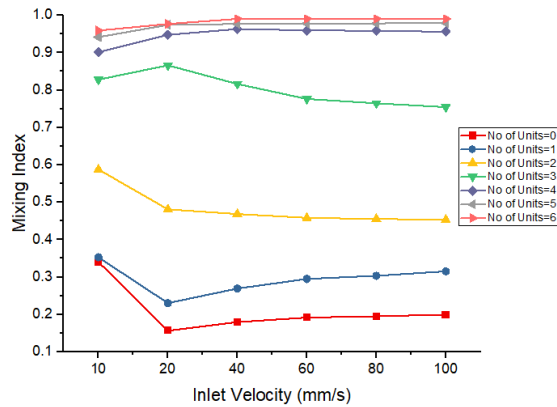

Fig 5. The influence of the number of mixing elements on the mixing performance.

To evaluate the mixing quality regarding the mixing elements, mass fraction contour plots have also been created at different cut planes perpendicular to the flow direction on the cross-sectional geometry of the KSM (Fig. 6). It is clear from the figure that the mass fraction distribution gradually becomes uniform after each mixing unit and the optimal mixing is achieved at outlet.
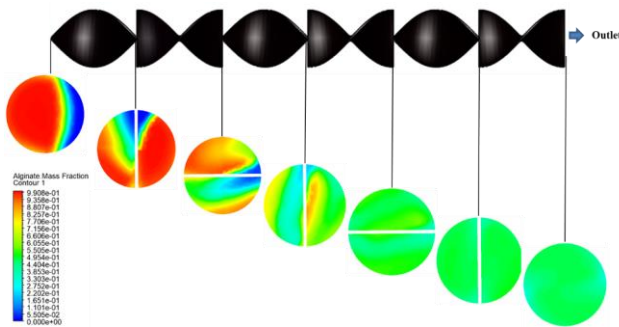

Fig 6. Mass fraction distribution of alginate (5%) at cross-sections after each mixing unit for 20 mm/s of inlet velocity.

3.3. Effect of shear-thinning behavior on the mixing process

According to Eq. (4), the apparent viscosity of power-law fluids increases by increasing the fluid consistency index (k). As the apparent viscosity increases the chaotic advection effect is weakened by viscous forces and the mixing system is susceptible to poor mixing [27]. To address the effect of viscosity on the degree of mixing, simulations were conducted considering solutions containing three different alginate concentrations (2%, 3%, and 5%) and fixed amount of gelatin (5%). The MI values were calculated at cross-sectional planes in the middle of the mixing chamber

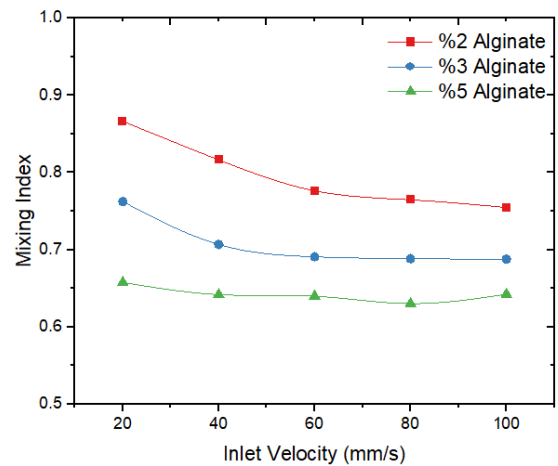(after 3rd mixing elements) for inlet velocities ranging from 20 mm/s to 100 mm/s (Fig. 7).

Fig 7. Effect of viscosity on the mixing performance for different alginate concentrations.

As presented in Table 2, solutions containing 5% of alginate exhibit the highest consistency index and the highest apparent viscosity value compared to the other alginate solutions. Therefore, for all inlet velocities, the lowest mixing index value was obtained for 5% alginate solutions, whereas the highest value was obtained for 2% of alginate solutions.

3.4. Effect of inlet velocity and shear-thinning behavior on pressure drop

In all considered simulations, static pressure was set to zero (P=0) at the outlet. The pressure drop was determined by calculating the difference between pressure values before the first mixing element and at 0.3 mm downstream of the last mixing unit (outlet). Pressure drop (ΔP) is computed through the six mixing units in the static mixers. Fig. 8a shows the calculated pressure drop values at various velocities ranging from 20 to 100 mm/s. As observed, ΔP value is very low for the low inlet velocities. However, it increases continuously for the higher inlet velocity values. The observed increase in ΔP could be attributed to an increase in the shear force, frictional losses, and inertial effects. The effect of shear-thinning behaviour on pressure drop was also evaluated considering different power-law parameters, $n = 0.2, 0.4, 0.6, 0.8$ and 1, and fluid consistency index of $k = 100$ Pa.s^n, while the inlet velocity was 100 mm/s for each inlet. The pressure drop values as a function of the power-law indices are illustrated in Figure 8b. As previously mentioned, the fluids exhibit a significant shear-thinning behaviour as the power-law index approaches to zero. The fluid viscosity decreases by increasing the shear rate and consequently, the fluids easily flow throughout the mixing channel. Therefore, this shear-thinning behaviour reduces the pressure drop in comparison to Newtonian fluids ($n = 1$). It was also reported that for shear-thinning fluids a higher mixing quality and a lower pressure drop were obtained compared to Newtonian fluids [29]. Similar results were also

obtained by [30]. One possible implication of this is that by assuming, for simplicity reasons, shear-thinning fluids as Newtonian fluids the pressure drop is underestimate. It is also important to note that relatively low-pressure value is needed to extrude the biomaterials.
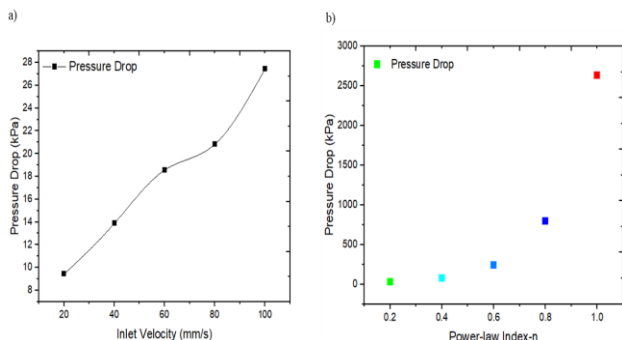

Fig 8. a) Effect of inlet velocity on the pressure drop; b) effect of power-law index on the pressure drop.

3.5. Effect of unequal inlet bulk velocities on mixing

Numerical analyses were also performed to investigate the capability to produce uniformly mixed homogenous functionally graded structures. In this case, the composition of the two materials being mixed was controlled by manipulating the inlet velocities. For example, to obtain a composition of 60% alginate, and 40% of gelatin, an inlet velocity of 300 mm/s was applied to alginate (inlet 1), and an inlet velocity of 200 mm/s was applied to gelatin (inlet 2). Different velocity ratios were considered as shown in Table 3. Fig. 9 shows the mass fraction contour plots at the outlets with corresponding mixing indices. Based on the results it can be concluded that applying different velocity ratios have no significant effect on the distributive mixing capacity of the mixer, suggesting that the proposed mixing channel is effective enough to ensure good mixing quality in case the inlet velocities of the fluids to be mixed are not equal. In addition, it is imported to note that by using different inlet velocity values it is possible to achieve a smooth transition of the flow with different material compositions.

Table 3. Inlet velocities for different fluid flow cases.

	Velocity (mm/s)	Velocity (mm/s)	Velocity ratio
Case	Inlet 1	Inlet 2	$V_1:V_2$
1	200	100	2:1
2	300	200	3:2
3	100	100	1:1
4	200	300	2:3
5	100	200	1:2

Fig 9. Mass fraction contour plots for different velocity ratios.

4. Conclusions

The flow behaviour of two miscible biomaterials were studied using computational fluid dynamics. A bifurcated shape printhead equipped with a KSM was designed and tested considering effective mixing conditions. The flow pattern inside the mixer was assessed considering non-Newtonian shear-thinning fluids at varying inlet velocities. All simulations were performed in a laminar regime and a power-law non-Newtonian model was applied. Numerical results showed that the inlet angle has not a remarkable effect on mixing quality and without a mixing unit inside the channel, the mixing index is quite low. At all the considered velocity values, the proposed printhead showed good mixing performance owing to the presence of chaotic advection regardless of velocity values. The apparent viscosity of power-law fluids increases by increasing the fluid consistency index, decreasing the chaotic advection effect. Therefore, the mixing system is susceptible to poor mixing. The effect of the shear-thinning behaviour on pressure drop was also investigated considering different power-law parameters. Results showed that the shear-thinning behaviour reduces pressure drop value compared to Newtonian fluids. Different velocity ratios from the inlets were applied and no significant effects on the distributive mixing capacity of the mixer was observed. However, different inlet velocity ratios allow to obtain a smooth transition of the flow from the mixing chamber.

Author's statement
Authors state no conflict of interest. Informed consent: Informed consent has been obtained from all individuals included in this study.

References

1. S. V. Murphy and A. Atala, "3D bioprinting of tissues and organs," *Nat. Biotechnol.*, vol. 32, no. 8, pp. 773–785, 2014.
2. B. Zhang, L. Gao, L. Ma, Y. Luo, H. Yang, and Z. Cui, "3D Bioprinting: A Novel Avenue for Manufacturing Tissues and Organs," *Engineering*, vol. 5, no. 4, pp. 777–794, 2019.
3. D. J. Odde and M. J. Renn, "Laser-guided direct writing for applications in biotechnology," *Trends Biotechnol.*, vol. 17, no. 10, pp. 385–389, 1999.
4. J. Malda *et al.*, "25th anniversary article: Engineering hydrogels for biofabrication," *Adv. Mater.*, vol. 25, no. 36, pp. 5011–5028, 2013.
5. K. Song, A. M. Compaan, W. Chai, and Y. Huang, "Injectable Gelatin Microgel-Based Composite Ink for 3D Bioprinting in Air," *ACS Appl. Mater. Interfaces*, vol. 12, no. 20, pp. 22453–22466, 2020.

6. J. C. Gómez-Blanco, E. Mancha-Sánchez, A. C. Marcos, M. Matamoros, A. Díaz-Parralejo, and J. B. Pagador, "Bioink temperature influence on shear stress, pressure and velocity using computational simulation," *Processes*, vol. 8, no. 7, pp. 1–18, 2020.

7. S. Kyle, Z. M. Jessop, A. Al-Sabah, and I. S. Whitaker, "'Printability'' of Candidate Biomaterials for Extrusion Based 3D Printing: State-of-the-Art,'" *Adv. Healthc. Mater.*, vol. 6, no. 16, pp. 1–16, 2017.

8. J. U. Lind *et al.*, "Instrumented cardiac microphysiological devices via multimaterial three-dimensional printing," *Nat. Mater.*, vol. 16, no. 3, pp. 303–308, 2017.

9. C. Chávez-Madero *et al.*, "Using chaotic advection for facile high-throughput fabrication of ordered multilayer micro- and nanostructures: Continuous chaotic printing," *Biofabrication*, vol. 12, no. 3, 2020.

10. I. Chiesa *et al.*, "Modeling the Three-Dimensional Bioprinting Process of β-Sheet Self-Assembling Peptide Hydrogel Scaffolds," *Front. Med. Technol.*, vol. 2, no. October, pp. 1–16, 2020.

11. S. Zhang, S. Vijayavenkataraman, W. F. Lu, and J. Y. H. Fuh, "A review on the use of computational methods to characterize, design, and optimize tissue engineering scaffolds, with a potential in 3D printing fabrication," *J. Biomed. Mater. Res. - Part B Appl. Biomater.*, vol. 107, no. 5, pp. 1329–1351, 2019.

12. I. P. Magalhães, P. M. de Oliveira, J. Dernowsek, E. B. Las Casas, and M. S. Las Casas, "Investigation of the effect of nozzle design on rheological bioprinting properties using computational fluid dynamics," *Rev. Mater.*, vol. 24, no. 3, 2019.

13. J. Emmermacher *et al.*, "Engineering considerations on extrusion-based bioprinting: interactions of material behavior, mechanical forces and cells in the printing needle," *Biofabrication*, vol. 12, no. 2, 2020.

14. I. Yu and R. Chen, "An experimental and numerical study on coaxial extrusion of a non-Newtonian hydrogel material," *J. Manuf. Sci. Eng. Trans. ASME*, vol. 143, no. 8, pp. 1–10, 2021.

15. T. Hozumi, S. Ohta, and T. Ito, "Analysis of the calcium alginate gelation process using a Kenics static mixer," *Ind. Eng. Chem. Res.*, vol. 54, no. 7, pp. 2099–2107, 2015.

16. J. Knoška *et al.*, "Ultracompact 3D microfluidics for time-resolved structural biology," *Nat. Commun.*, vol. 11, no. 1, pp. 1–12, 2020.

17. B. W. Nyande, K. Mathew Thomas, and R. Lakerveld, "CFD Analysis of a Kenics Static Mixer with a Low Pressure Drop under Laminar Flow Conditions," *Ind. Eng. Chem. Res.*, vol. 60, no. 14, pp. 5264–5277, 2021.

18. R. P. Chhabra and Richardson, "Chapter 1. Non-Newtonian fluid behaviour," *Non-Newtonian Flow Appl. Rheol. Eng. Appl.*, p. 536, 2011.

19. A. B. Metzner, "Non-Newtonian Fluid Flow Relationships between Recent Pressure-Drop Correlations," *Ind. Eng. Chem.*, vol. 49, no. 9, pp. 1429–1432, 1957.

20. S. Soman, "Study of effects of design modification in static mixer geometry and its applications," *Univ. Waterloo*, 2016.

21. N. Ait Mouheb, D. Malsch, A. Montillet, C. Solliec, and T. Henkel, "Numerical and experimental investigations of mixing in T-shaped and cross-shaped micromixers," *Chem. Eng. Sci.*, vol. 68, no. 1, pp. 278–289, 2012.

22. E. Fourcade, R. Wadley, H. C. J. Hoefsloot, A. Green, and P. D. Iedema, "CFD calculation of laminar striation thinning in static mixer reactors," *Chem. Eng. Sci.*, vol. 56, no. 23, pp. 6729–6741, 2001.

23. H. Meng, X. Jiang, Y. Yu, Z. Wang, and J. Wu, "Laminar flow and chaotic advection mixing performance in a static mixer with perforated helical segments," *Korean J. Chem. Eng.*, vol. 34, no. 5, pp. 1328–1336, 2017.

24. 1 Rubens Maciel Filho2 Rodrigo Alvarenga Rezende, 1, 2 Paulo Jorge Ba´rtolo, 1 Ausenda Mendes, "Rheological Behavior of Alginate Solutions for Biomanufacturing," *J. Appl. Polym. Sci.*, vol. 116, no. 5, pp. 2658–2667, 2010.

25. S. Karaman, E. Cengiz, A. Kayacier, and M. Dogan, "Exposure to air accelerates the gelation of gelatin: Steady and dynamic shear rheological characterization to see the effect of air on the strength of gelatin gel," *Int. J. Food Prop.*, vol. 19, no. 4, pp. 721–730, 2016.

26. Y. Zhang, Y. Hu, and H. Wu, "Design and simulation of passive micromixers based on capillary," *Microfluid. Nanofluidics*, vol. 13, no. 5, pp. 809–818, 2012.

27. D. Patel, F. Ein-Mozaffari, and M. Mehrvar, "Effect of rheological parameters on non-ideal flows in the continuous-flow mixing of biopolymer solutions," *Chem. Eng. Res. Des.*, vol. 100, pp. 126–134, 2015.

28. E. L. Paul, V. a Atiemo-obeng, and S. M. Kresta, *HANDBOOK OF INDUSTRIAL MIXING Edited by*. 2004.

29. S. Liu, A. N. Hrymak, and P. E. Wood, "Laminar mixing of shear thinning fluids in a SMX static mixer," *Chem. Eng. Sci.*, vol. 61, no. 6, pp. 1753–1759, 2006.

30. A. S. Lobasov and A. V. Minakov, "Analyzing mixing quality in a T-shaped micromixer for different fluids properties through numerical simulation," *Chem. Eng. Process. Process Intensif.*, vol. 124, no. April 2017, pp. 11–23, 2018.